Biomaterials Advances 152 (2023) 213485

Contents lists available at ScienceDirect

Biomaterials Advances

journal homepage: www.journals.elsevier.com/materials-science-and-engineering-c

In-vitro investigation of endothelial monolayer retention on an inflow VAD cannula inside a beating heart phantom

Konstantinos Magkoutas [a,1], Nafsika Chala [b,1], Xi Wu [c], Dimos Poulikakos [b], Edoardo Mazza [c,d], Mirko Meboldt [a], Volkmar Falk [e,f,g], Aldo Ferrari [b], Costanza Giampietro [c,d,*], Marianne Schmid Daners [a,**]

[a] Product Development Group Zurich, Department of Mechanical and Process Engineering, ETH Zurich, Zurich, Switzerland
[b] Laboratory of Thermodynamics in Emerging Technologies, Department of Mechanical and Process Engineering, ETH Zurich, Zurich, Switzerland
[c] Experimental Continuum Mechanics, Department of Mechanical and Process Engineering, Institute for Mechanical Systems, ETH Zurich, Zurich, Switzerland
[d] Experimental Continuum Mechanics, EMPA, Dubendorf, Switzerland
[e] Department of Cardiothoracic and Vascular Surgery, German Heart Center Berlin, 13353 Berlin, Germany
[f] Clinic for Cardiovascular Surgery, Charité – Universitätsmedizin Berlin, 13353 Berlin, Germany
[g] Department of Health Sciences and Technology, ETH Zurich, 8093 Zurich, Switzerland

ARTICLE INFO

Keywords:
Ventricular assist devices (VADs)
Endothelialization
Endothelial monolayer
Thrombosis
Heart phantom
Dynamic testing

ABSTRACT

Ventricular assist devices (VADs) provide an alternative solution to heart transplantation for patients with end-stage heart failure. Insufficient hemocompatibility of VAD components can result in severe adverse events, such as thromboembolic stroke, and readmissions. To enhance VAD hemocompatibility, and avoid thrombus formation, surface modification techniques and endothelialization strategies are employed.

In this work, a free form patterning topography is selected to facilitate the endothelialization of the outer surface of the inflow cannula (IC) of a commercial VAD. An endothelialization protocol for convoluted surfaces such as the IC is produced, and the retainment of the endothelial cell (EC) monolayer is evaluated. To allow this evaluation, a dedicated experimental setup is developed to simulate realistic flow phenomena inside an artificial, beating heart phantom with a VAD implanted on its apex. The procedural steps of mounting the system result to the impairment of the EC monolayer, which is further compromised by the developed flow and pressure conditions, as well as by the contact with the moving inner structures of the heart phantom. Importantly, the EC monolayer is better maintained in the lower part of the IC, which is more susceptible to thrombus formation and may therefore aid in minimizing the hemocompatibility related adverse events after the VAD implantation.

1. Introduction

Mechanical circulatory support with ventricular assist devices (VADs) is an established alternative to heart transplantation. It contributes to mitigate the shortage of available donor organs and thus allows for better management of end-stage heart failure patients [1,2]. In addition, VAD implantation constitutes the main available lifeline for patients who do not qualify for transplantation due to comorbidities and general health conditions.

Over the last decade, the use of VADs has been significantly increased, while their deployment strategy has shifted from bridge-to-transplantation (BTT) to destination therapy (DT), with DT accounting for 73 % of all VAD implantations in 2019 [3]. This paradigm reflects the evolution in patient selection, implantation procedure, post-operative patient treatment, and most importantly, the predominant use of hybrid- and fully-levitated continuous flow turbodynamic VADs (cfVADs) that resulted in improved survival rates and quality-of-life [1,3–5]. Currently, the one year survival rate for patients receiving a VAD approaches that of heart transplantation [3].

Based on these results and the demographics of the Western

* Correspondence to: C. Giampietro, Experimental Continuum Mechanics, Department of Mechanical and Process Engineering, Institute for Mechanical Systems, ETH Zurich, Zurich, Switzerland.
** Corresponding author.
E-mail addresses: costanza.giampietro@empa.ch (C. Giampietro), marischm@ethz.ch (M. Schmid Daners).
[1] These authors contributed equally to this work.

https://doi.org/10.1016/j.bioadv.2023.213485
Received 31 December 2022; Received in revised form 21 May 2023; Accepted 26 May 2023
Available online 29 May 2023

population, the number of VAD implantations is expected to steadily grow in the near future. However, the high rate of VAD-associated adverse events (AEs), especially in the long term, remains a great challenge [3,6,7]. Although the fully-levitated cfVADs support the mitigation of the AEs, hemocompatibility-related AEs, including nonsurgical bleeding and thromboembolic events that lead to stroke (ischemic or hemorrhagic) or pump thrombosis with the consequence of pump malfunction, continue to be the most frequent causes for patient readmission [8–11]. The thromboembolic events are believed to originate from thrombus depositions and growth in the vicinity of the aortic valve, outflow graft, VAD impeller and, most importantly, the luminal surface of the VAD inflow cannula (IC) [6,9,12–16]. At the IC (Fig. 1), the risk of clot formation is aggravated by the substantial injury of the endothelium, the stagnant-flow, and the hypercoagulability triggered by the higher protein absorption of the luminal surface of the IC [14,17,18]. Attempts to control this risk exploit different options for surface modification of the luminal area [19]. In some VADs, the IC interface has been modified with sintered titanium microspheres that aim at controlling the tissue ingrowth [13,15,20]. Despite some improvement [13], anticoagulation treatment continues to be necessary after the implantation of a VAD, exposing the recipients to high risk of bleeding [9,11].

The long-term, complication-free integration of VADs is the promise of alternative strategies, which aim at fully restoring the homeostasis of the endothelial layer of the heart tissue upon implantation. The main purpose is to eliminate the discontinuity created by the IC and avoid the direct contact between the IC surface and blood. This shall be achieved by creating the conditions to reconstitute and maintain an autologous functional endothelium – the process of endothelialization – on the IC surfaces interacting with blood [18,21].

Viable endothelialization protocols dedicated to the IC must consider the specific challenges associated with the implantation procedure and the local hemodynamic conditions created by the function of the blood pump. The VAD actuation and the architecture of its surface, create regions of disturbed flow, with non-physiological wall shear stress (WSS) and flow recirculation [17]. In this hemodynamic environment, endothelial cells (ECs) must be able to firmly adhere to the substrate and establish mature cell-to-cell junction complexes, that ensure the barrier function of the monolayer. Among these, the adherens junctions are composed by a multi protein complex linked to the actin cytoskeleton. One of their key components is the vascular endothelial cadherin (VE-cadherin, [22]), that is used to identify connected monolayers of ECs by its junctional localization and that, through its interaction with actin-binding proteins, regulates actin remodeling [23].

We have previously demonstrated that rationally developed topographical modifications, in the form of micron sized topographical features, can interact with the sweeping flow to extend the range of viable hemodynamic conditions, and support the survival of cells in otherwise prohibitive conditions [21,24–27]. The implementation of such protective geometries on non-planar synthetic substrates can be obtained by means of dedicated self-assembly protocols, harnessing the process of breath figure formation in a facile and free form structuring approach [28]. Here, the previously established free form patterning method of breath figures [28] is modified and employed on the outer surface of the HeartMate3 (HM3, Abbott, USA) VAD IC to enhance endothelialization. The retainment of the EC monolayer is investigated under realistic flow phenomena by exploiting a newly developed experimental setup. In this setup, a HM3 VAD is implanted on the apex of an artificial, beating heart phantom, enabling the simulation of different VAD support scenarios by changing the actuation conditions. The retainment of the EC monolayer is also correlated to the position of the cannula inside the left ventricle, highlighting the influence of the moving papillary structures that interfere with the IC surface.

2. Materials and methods

2.1. Cell culture

Primary human umbilical vein endothelial cells (HUVECs), neonatal, and pooled were purchased from Promocell (#C-12203, Promocell, Germany) and cultured as recommended by the supplier. Cells were cultured in Endothelial Cell Growth Medium (#C-22010, Promocell, Germany), which was supplemented with 2 % fetal calf serum, endothelial cell growth supplement 0.004 mL/mL, epidermal growth factor 0.1 ng/mL, basic fibroblast growth factor 1 ng/mL, heparin 90 μg/mL and hydrocortisone 1 μg/mL. Moreover, 1 % v/v penicillin-streptomycin (#15140122, Life Technologies, ThermoFisher Scientific, USA) was added to the medium. HUVECs were expanded in the presence of 20 % v/v fetal bovine serum (#10270106, Life Technologies, ThermoFisher Scientific, USA) and were maintained at 37 °C and 5 % CO_2. All experiments were performed using HUVECs with less than six passages *in vitro* and low serum medium (2 %).

To enhance endothelial cell adhesion, ICs were coated with glutaraldehyde-crosslinked gelatin as previously reported [29]. The ICs were incubated for at least 1 h at 37 °C with 1.5 % gelatin followed by a crosslinking with 2 % glutaraldehyde solution for 15 min at room temperature (RT). The glutaraldehyde was replaced by 70 % ethanol. After 1 h, five washes with phosphate-buffered saline (PBS) followed by overnight incubation with PBS containing 2 mM glycine at 37 °C were performed. Before cell seeding, ICs were washed five times with PBS.

2.2. Inflow cannula surface topography

The application process of the “Breath Figures (BF)” surface topography was done similarly to our previously published protocol [28]. To adapt the coating protocol to the geometry of the IC, the dip coating method was used to create a silicone coating. Specifically, the IC was

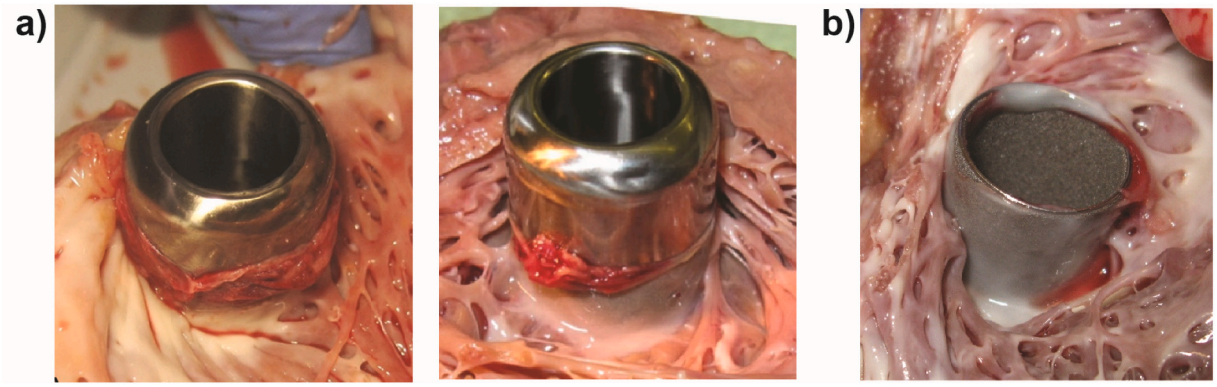

Fig. 1. Inflow cannula (IC) regions highly susceptible to thrombus formation. **a)** HVAD (Medtronic, Ireland) inflow cannula (Image source: Retrieved from Kaufmann et al. [15]), **b)** HeartMate3 (Abbott, USA) inflow cannula (Kaufmann, F. 2021. Photograph taken at Berlin by Friedrich Kaufmann. At: German Heart Center Berlin).

dipped into a liquid silicone bath (Fig. 2b) that was produced by mixing two portions of RTV4420 A + B (Elkem silicone, France) in a 1:1 ratio. Immediately after, the IC was transported to a cylindrical support base with an external diameter that equals the one of the IC (Fig. 2c). The excessive silicone (overflow) was smoothly guided to the support base, leaving a thin and homogenous silicone coating layer on the IC.

To pattern the silicone surface and ensure maximum overflow time, the RT curing protocol [28] was used. In detail, the silicone coating was cured at RT (23 ± 1 °C) for 125 min. The ICs were then rapidly cooled at 4 °C for 5 min to facilitate the droplet nucleation. Once the nucleation phase was complete, the ICs were transferred to a dedicated environmental chamber at 37 °C and 100 % relative humidity (RH), sustained for 25 min by a heated water bath. The orientation of the IC was as indicated in Fig. 2d to ensure that the coated part was in contact only with the humid air. After the patterning, the silicone coating in the luminal surface of the IC was removed. The temperature and the humidity history throughout the fabrication process are summarized in Fig. 2e. Compared to the original protocol the cooling temperature was increased from −20 °C to 4 °C, the curing temperature was increased from 32 °C to 37 °C and the curing time was decreased from 30 min to 25 min [28].

To characterize the BF patterns, a VK-X200 3D laser scanning confocal microscope (Keyence, Japan) [30] was used to generate surface heightmaps with 100 nm resolution in the z axis. Tilt and curvature-corrected height data were processed by an in-house MATLAB (MathWorks Inc., USA) code, which detected the individual wells, measured their diameter, depth, and inter-well center-to-center distance. Specifically, the depth was computed by the height difference between the center point of the well and the flat area outside the well. The center-to-center distance was calculated as the distance between the centers of two neighboring wells. Additionally, in order to investigate the consistency of the topography characteristics along the axial direction of the IC, a local scan with a size of 537 μm × 783 μm and a large area scan with a size of 537 μm × 4480 μm were performed. By comparing the local and the large area scans, the local scan was validated as representative of the topography achieved and adequate to perform its characterization. Thus, local scans were executed to characterize the topography for all the ICs used in the experiments.

2.3. Endothelial cell seeding protocol

The patterned ICs were incubated in 70 % ethanol for 30 min at RT and then were let to dry. A step of oxygen plasma (100 W for 30 s, 1 ± 0.2 mbar) was performed to increase the hydrophilicity of the surface, followed by the glutaraldehyde-crosslinked gelatin coating (described in section 2.1).

To achieve a homogeneous seeding along the IC, a custom-made holder from biocompatible resin (DS-3000, DWS Srl, Italy) was 3D printed (XFAB 2500HD DWS Srl, Italy). This holder allowed to perform the seeding process in four steps, by ensuring fixed, 90 ° rotations of the cannula. In each step, a quarter of the total number of endothelial cells (ECs) were seeded along the long axis of the IC, followed by a 20-min

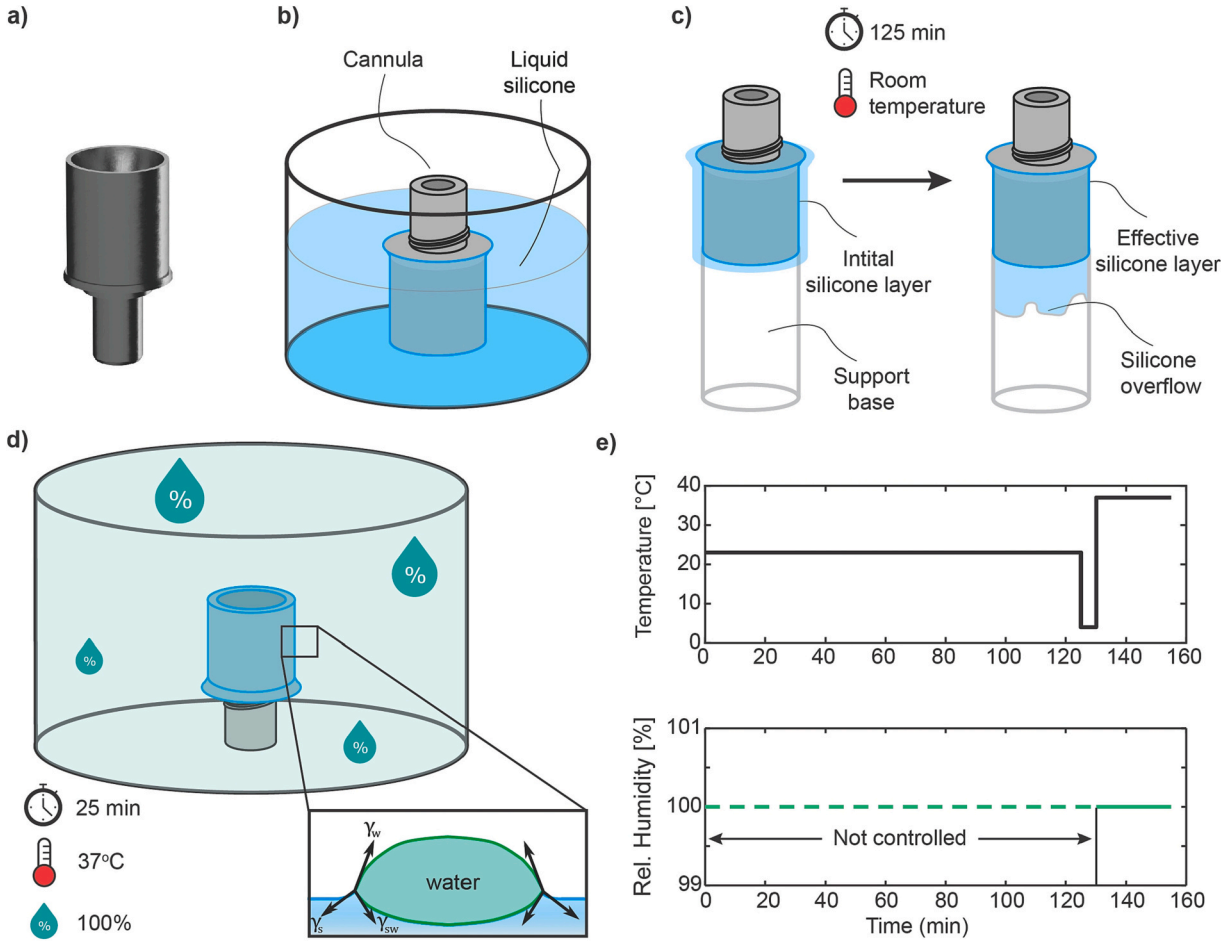

Fig. 2. Fabrication process of the Breath Figures (BF) topography [28]. **a)** Render of the original inflow cannula. **b)** Illustration of the dip coating process. **c)** Illustration of the curing process. **d)** Illustration of the patterning process. **e)** Evolution diagrams of the target temperature and target humidity throughout the fabrication process. The dashed line indicates that the humidity was not controlled during the dip coating, nor during the curing and cooling processes (first 130 min).

waiting period with the cannula being secured in its position. As a next step, the IC mounted on the holder was inserted in the incubator at 37 °C and 5 % CO_2 for 20 min, ensuring the attachment of the cells on the specific side of the IC. These sequential steps were repeated for the remaining three quarters of the cannula to complete the seeding process. Notably, to guarantee an EC adherence to the convex surface of the IC adequate to form a monolayer, the seeding density was 13.8×10^4 cells/cm^2, which is three times the density required to prepare a confluent monolayer on a flat surface [31]. The adherent cells were cultured for three days to achieve a mature monolayer prior the experiments [29].

2.4. Immunostaining and imaging

The coated IC was immersed in 4 % paraformaldehyde in PBS (#28908, Thermo Scientific, USA) for 15 min at RT to fix the cells. The silicone layer with the cells was carefully removed from the IC and laid flat to perform the immunostaining. Cells were permeabilized using PBS with 0.5 % Triton X-100 (#T8787, Sigma Aldrich, USA) for 10 min and then incubated in a blocking solution of PBS with 5 % bovine serum albumin (BSA) (#A6003, Sigma Aldrich, USA) for 1 h at RT. Subsequently, the silicone layers were incubated with the primary antibody of rabbit anti-vascular endothelial cadherin (VE-cadherin, 1:200, #D87F2, Cell Signaling Technology, USA) diluted in blocking buffer at 4 °C overnight. After rinsing the silicone layers three times with PBS, they were incubated with the secondary antibody Alexa Fluor 488 donkey anti-rabbit (1:200, #A21206, Invitrogen, USA), Phalloidin-TRITC (Actin, 1.25 μg/mL, #P1951, Sigma Aldrich, USA), and the nuclear staining reagent DAPI (1:1000, #62248, Thermo Scientific, USA) diluted in blocking buffer for 45 min at RT. Finally, the silicone layers were rinsed three more times with PBS and then they were mounted with Fluoroshied (#F6182, Sigma Aldrich, USA).

For the imaging of the immunostained silicone layers, an inverted Nikon-Ti spinning disk confocal microscope (Nikon, Japan) equipped with an Andor DU-888 camera (Oxford Instruments, UK) and a pE-100 LED illumination system (CoolLED Ltd., UK) were used. Fluorescence images were acquired with the 10×, 0.3 NA air objective (Plan Fluor, Nikon, Japan) and the 20×, 0.75 NA air objective (Plan Apo, Nikon, Japan).

2.5. Experimental setup for in-vitro testing

2.5.1. Realistic, beating heart phantom

The heart phantom aimed to accurately imitate the movement of the beating heart and, hence, enable the development of realistic flow phenomena in the vicinity of the IC of the VAD. To achieve this, the first step was the acquisition of the three-dimensional (3D) geometry of a dilated heart. More precisely, the different layers of magnetic resonance (MR) cross sectional images retrieved from a heart failure patient (Fig. 3a) were stacked together to generate the 3D model of the entire heart in a computer-aided design (CAD) format (Geomagic Design X, Artec3D, Luxembourg). This CAD model was further processed to remove the left and right atria, as well as to incorporate the necessary openings for the inflow and outlet ports of the heart, and the insertion of the IC.

Based on this 3D model, the mold and core structures were produced by subtracting the 3D model from a solid body, to enable the manufacturing of the heart phantom with the lost-wax casting technique [32]. The mold structures were printed from polylactic acid (PLA) using a fused deposition molding (FDM) 3D-printer (Prusa MK3S, Prusa Research a.s., Czech Republic) and the inner surfaces were treated with XTC-3DTM (Smooth-on) to eliminate the layered topology resulting from the FDM process. The cores, representing the cavities of the left and right ventricles, were 3D printed from water dissolvable polyvinyl acetate (PVA). The mold structures and the cores were mounted together and the remaining cavities forming the walls of the heart phantom were filled with EcoflexTM 00–50 (Smooth-on) silicone that offers high elasticity and high durability in cyclic fatigue. Before injecting the silicone with syringes into the mold form, the silicone was de-aired with a vacuum pump to reduce the amount and size of air bubbles in the liquid silicone, hence avoiding the formation of small holes in the heart phantom. The molded silicone was left at RT for 24 h to cure and after disassembling the mold structures, the heart phantom was submersed for 5 days in a water bath at 80 °C to dissolve the cores. Finally, to allow a tight connection of the VAD on the heart phantom, a titanium ring was glued with silicone glue (#555–588, RS, UK) at the insertion area of the inlet cannula.

2.5.2. Experimental setup overview

The experimental setup (Fig. 3b) used for the assessment of the retention of the EC monolayer, mimicked the flow conditions of a dilated heart supported with a VAD. In the setup, the HM3 VAD with the modified IC was mounted on the apex area of the realistic heart phantom through custom-made titanium rings. The inlet port of the left ventricle of the heart phantom was connected *via* a hydraulic line of biocompatible tubes (Tygon®, France) to an air-trap and then to the 3D printed bellows. A linear motor (LinMot, Switzerland) was deployed to deform the bellows and, hence, the change in the bellows' volume was directly translated to change in the volume of the left ventricle of the silicone heart phantom. By defining the reference trajectory of the linear motor, the desired contractility level was achieved. The outlet port of the left ventricle of the heart phantom and the VAD outlet were connected with a Y-type connector to form the return line. Two unidirectional valves were used to emulate the mitral and aortic valves and, consequently, to avoid backflow. The hydraulic line was equipped with a flow sensor (Sonoflow, Sonotec, Germany) after the Y-type connector and two pressure sensors (TruWave, Edwards Lifesciences, California), at the inlet and the outlet of the heart phantom. To preserve the endothelial cells, CO_2 was administered with a constant flow of 9 L/h, while the entire heart phantom with the VAD was immersed in a water bath that was maintained at 37 °C with a heating element (Julabo, Germany). All sensors were connected to an NI-DAQ-USB6210 (National Instruments, USA) with sampling frequency of 1 kHz and the data were continuously recorded with a personal computer *via* a custom script in MATLAB.

2.5.3. Experimental conditions and protocol

To investigate the retention of the EC monolayer under various clinical scenarios, the pulsatility level of the heart phantom and the rotational speed of the VAD were manipulated. Specifically, by varying the stroke length of the linear motor between 0 and 30 mm and the rotational speed of the VAD between 0 and 4000 rpm, the scenarios of low- and high-pulsatility with no- or low-VAD support were imitated. The exact values and their combinations are provided in Table 1. The execution of each experiment (ID) was three-fold, while the effective duration was 8 h. In Fig. 4, the flow measured at the VAD outlet, the cumulative flow produced from the left ventricle and the VAD, as well as the pressure at the inlet and outlet of the left ventricle are illustrated.

2.6. Setup preparation protocol

Since the setup cannot be positioned in a sterile environment, the entire system was prepared before each experiment. In detail, the VAD (without the inflow cannula) was mounted on the heart phantom and connected to the hydraulic line of the setup. 70 % ethanol was run through the system for 30 min and after the circuit was emptied, it was washed three times with PBS. Then, the heart phantom together with the VAD and their support structure were disconnected from the rest of the setup and the VAD was dismounted. The heart phantom was filled with pre-warmed medium, the inflow cannula with the endothelial monolayer was inserted in the VAD and mounted back on the heart phantom. The mounting process was performed carefully to avoid touching the outer surface of the coated IC to the ring of the heart phantom. Afterwards, they were connected again to the rest of the setup, the circuit was

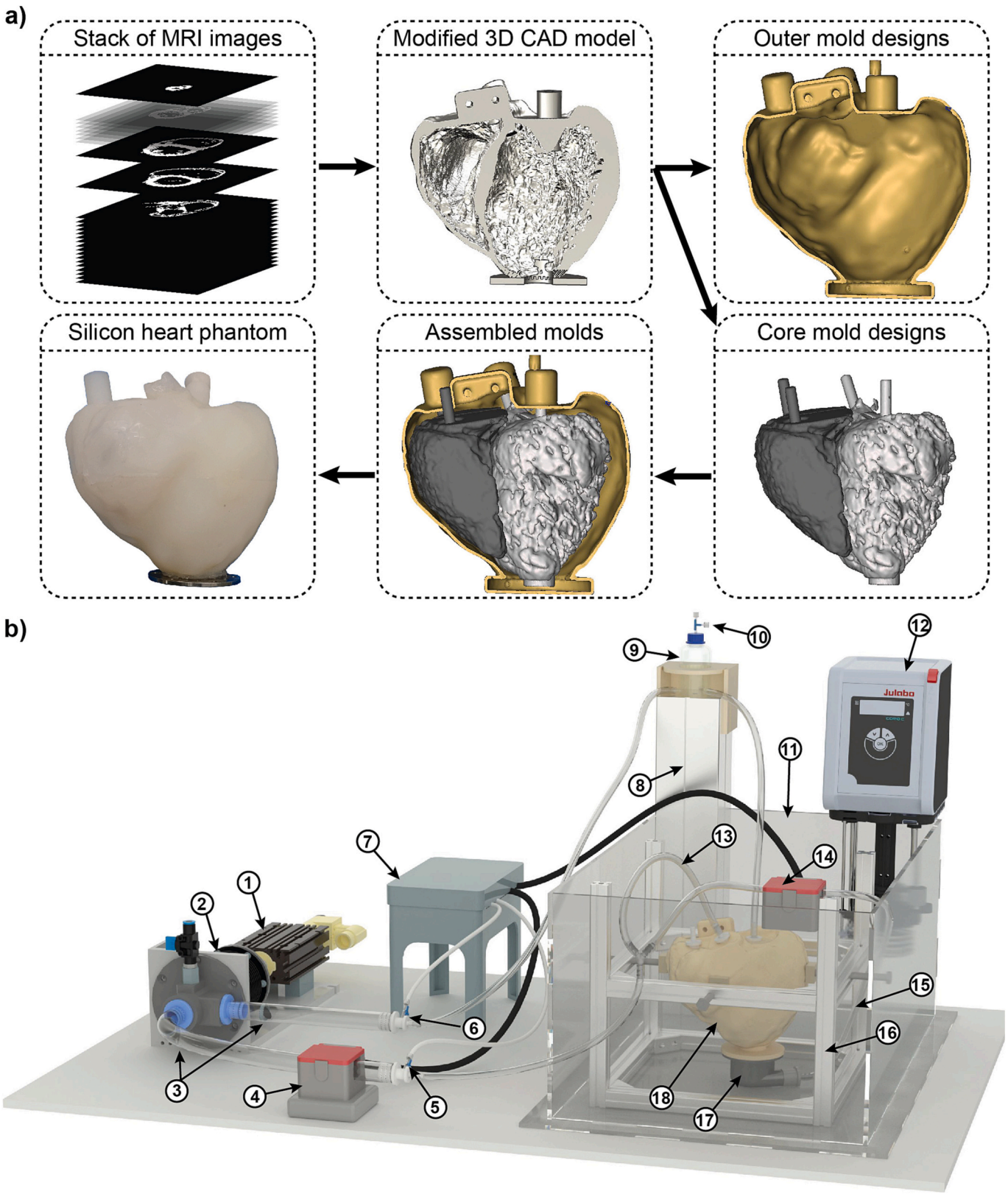

Fig. 3. Schematic of the experimental setup. **a)** Manufacturing process for the development of the realistic, beating heart phantom. **b)** Setup overview: 1) Linear motor, 2) Bellows, 3) Unidirectional valves, 4) Flowmeter measuring the total cardiac output (left ventricular flow & VAD flow), 5) Outlet pressure sensor port, 6) Inlet pressure sensor port, 7) Electronics' box, 8) Column for hydrostatic pressure control, 9) Air-trap, 10) CO_2 admission port, 11) Water tank, 12) Heating element, 13) Hydraulic line for left ventricular outlet, 14) Flowmeter measuring VAD flow, 15) Hydraulic line for VAD outlet, 16) Support structure for heart phantom, 17) VAD, and 18) Realistic heart phantom.

Table 1
Experimental settings to investigate the retention of the EC monolayer under various clinical scenarios.

ID	Scenario	Stroke length (mm)	Rotational speed (rpm)
0	Static	0	0
1	Low pulsatility / no-VAD support	15	0
2	High pulsatility / no-VAD support	30	0
3	Low pulsatility / low-VAD support	15	4000

filled with medium, CO_2 administration started, and the water bath was filled with pre-warmed water. The experimental conditions were defined based on the experiment ID (Table 1) and the experiment was initiated.

At the end of each experiment, the heart phantom together with the VAD and the support structure were disconnected from the rest of the setup. The disconnected part was filled with medium. The VAD was carefully dismounted from the heart phantom to avoid touching the outer surface of the coated IC to the ring of the heart phantom. The orientation of the IC was marked, and the IC was removed from the VAD and immersed in 4 % paraformaldehyde in PBS for fixation. Then, the medium was removed from the setup, and the circuit was washed with 70 % ethanol.

2.7. Quantification of endothelial cell retention

To quantify the retention of the EC monolayer on the cannulas, immunofluorescent images were used. More specifically, the full area of the recovered silicone layers was scanned with the 10× objective (Step 1; Fig. 5a), selecting the 'Custom Multipoint Large Image' function of the NIS software (Nikon, Japan). Then, with the 'Stitch Multipoint to Large Image' function of the NIS software, the individual images were stitched together to generate the large-scale images of the silicone layers (Step 2; Fig. 5b). In three steps, a quality-map showing the areas with a connected monolayer, with an impaired monolayer and without cells was generated. First, the immunofluorescent images of VE-cadherin and actin were used to define the areas with the connected monolayer (Step 3; Fig. 5c). Then, the image with the DAPI signal was used to define the areas where cells were present, but the monolayer was impaired (Step 4; Fig. 5d). Finally, the individual images were scanned to verify the acquired quality-map and fill in the details (Step 5; Fig. 5e). To quantify the percentage of each condition, the quality-maps were imported in MATLAB and the percentage of each color in the quality-map was computed.

In order to establish a relationship between the quality of the EC monolayer and the location of the IC and the surrounding tissue within the heart phantom, the quality-maps of the EC monolayers were incorporated into the 3D CAD model of the IC. The modified CAD model of the heart phantom (Fig. 3a) was imported in Fusion 360 (Autodesk, USA). Then, a simplified model of the VAD with an accurate IC geometry was created and positioned inside the model of the heart phantom. The position and orientation of the IC was carefully adjusted to match the experimental details. The quality-map of the EC monolayer was placed on the external surface of the CAD model of the IC by modifying the 'Appearance' attribute of the surface of the CAD model. To ensure that the radial position of the quality map was correct, an anchor point was marked at the end of the experimental procedure on the IC. This position was identified on the CAD model of the IC and by adjusting the offset in the X- and Y-axis of the quality map in the CAD model, the anchor point was aligned to the one on the experiment. Finally, the function 'Section Analysis' was used to generate the four different cross-sectional views of the integrated model.

2.8. Statistical analysis

The Shapiro-Wilk test was used to evaluate the normality of the data. For normally distributed data, the *t*-test was performed, while for non-normally distributed data, the Mann–Whitney *U* test was performed. For all tests, specificity of 0.05 was used. All statistical analysis was performed in Origin [33].

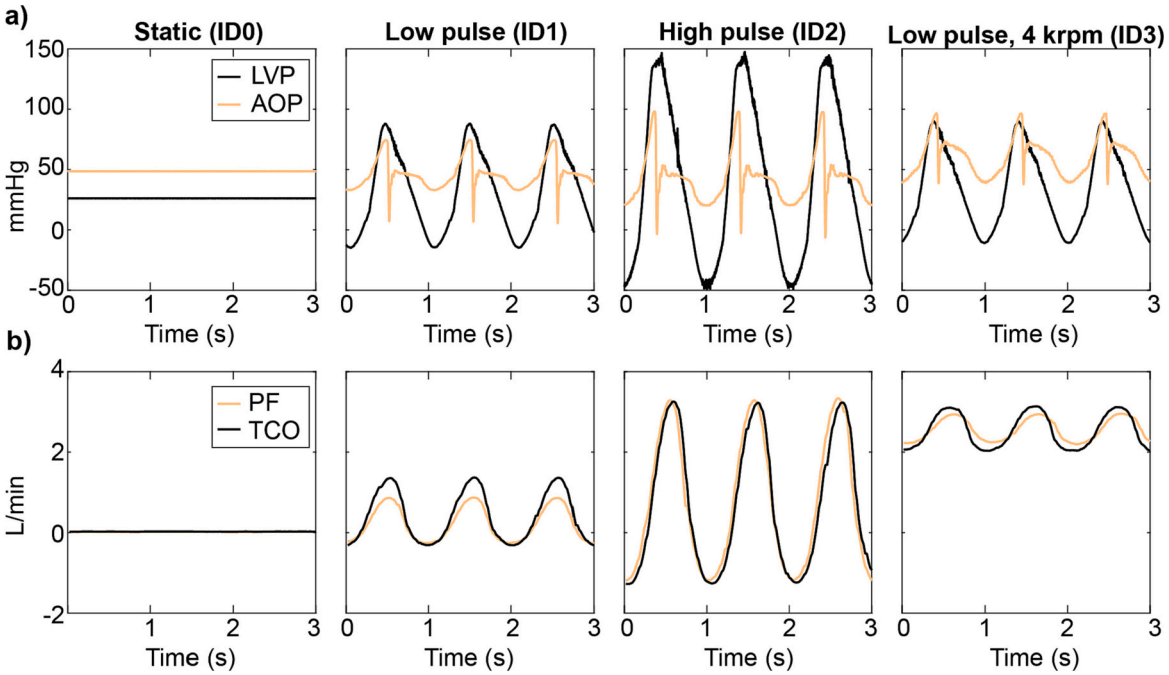

Fig. 4. Hemodynamic conditions under the simulated scenarios. **a)** Pressure waveforms, **b)** Flow waveforms. *LVP, left ventricular pressure; AOP, arterial pressure; PF, pump flow; TCO, total cardiac output (summation of left ventricular flow and pump flow).*

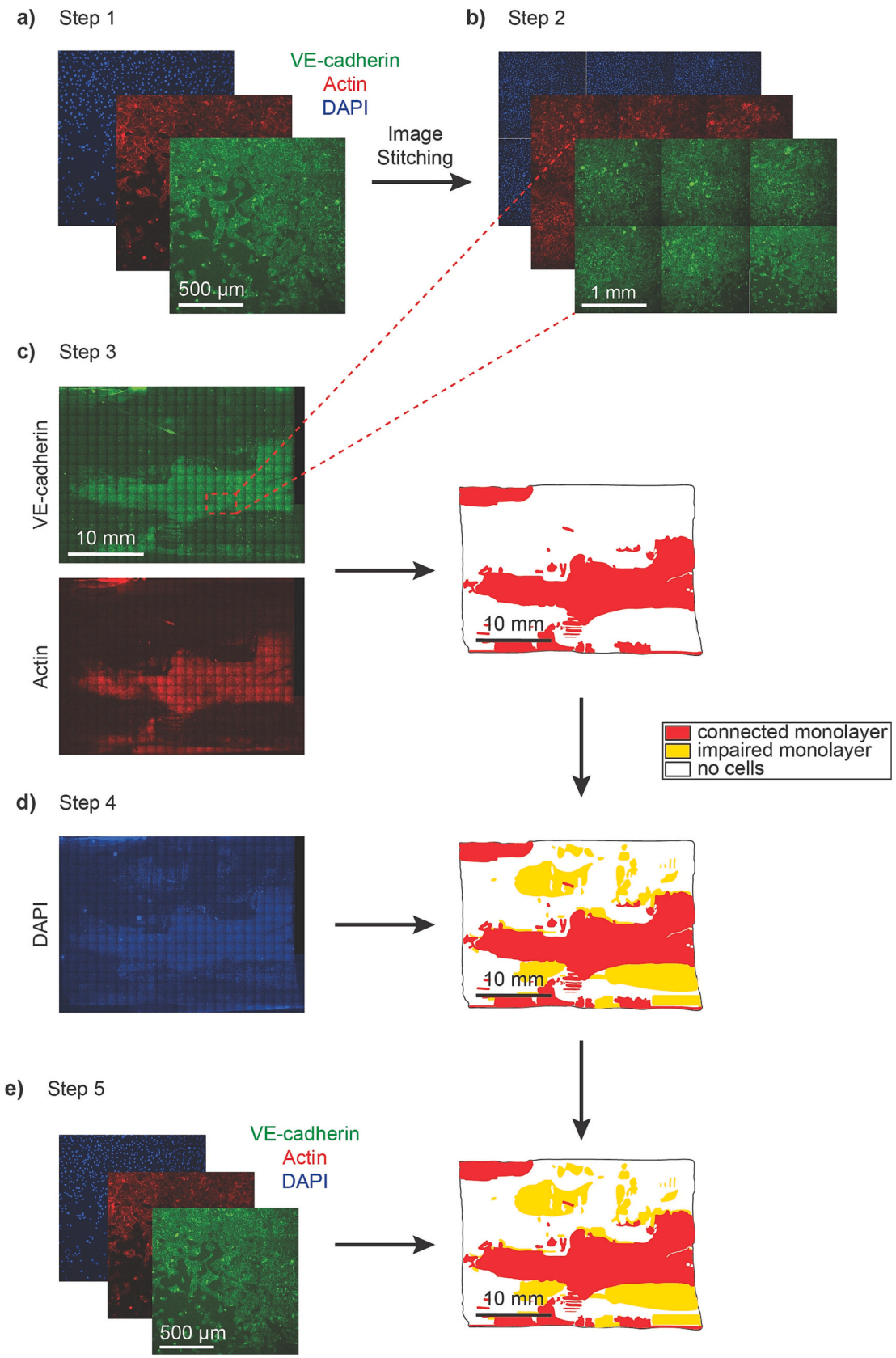

Fig. 5. Overview of the steps for the endothelial retention quantification. **a)** Step 1: Individual images of VE-cadherin, actin and DAPI. **b)** Step 2: Stitching of individual images to generate large scale images. **c)** Step 3: Large scale images of VE-cadherin and actin are used to identify the areas of the quality-map with connected monolayer. **d)** Step 4: Large scale images of DAPI are used to identify the areas of the quality-map with impaired monolayer. **e)** Step 5: Individual images of VE-cadherin, actin and DAPI are used to scan and verify the generated quality-map.

3. Results

3.1. Surface topography application on the inflow cannula

The modification of the surface topography protocol by adjusting the cooling temperature and curing time resulted in topography characteristics on the outer surface of the IC similar to those previously reported for planar and curved surfaces [28]. These characteristics are provided on Fig. 6, where it is shown that among the various experiments, the mean diameter of the topography was 67.9 ± 6.3 μm, the mean inter-well center-to-center distance was 118.2 ± 10.2 μm and the mean depth of the wells was 6.5 ± 1.0 μm.

The topography characteristics along the axial direction of the IC were further assessed by comparing the scans of a local and a large surface area, as described in Section 4.2. As shown in Fig. 6c, among the two scans of different scale, the topography distributions were similar for all the investigated topography characteristics, indicating the consistency of the topography along the axial direction of the IC.

3.2. Dynamic flow conditions

The versatility of the developed experimental setup (Fig. 3b) to simulate different clinical scenarios is demonstrated in Fig. 4, where the hemodynamic conditions developed during several possible scenarios are provided. In static experimental conditions (ID0), the left ventricular pressure (LVP) was fixed at 30 mmHg, while the aortic pressure (AOP) was at 50 mmHg. In the low pulsatility scenario (ID1), the LVP ranged between −10 mmHg and 90 mmHg during diastole and systole, respectively. The AOP ranged between 30 mmHg and 75 mmHg during diastole and systole, respectively, with an instantaneous pressure drop to 7 mmHg due to the closure of the aortic valve. During the same experimental settings, the mean total cardiac output was 1.2 L/min. In the high pulsatility scenario (ID2), during diastole and systole the LVP and AOP ranged between −50 mmHg and 150 mmHg, and between 25 mmHg and 100 mmHg, respectively. The mean total cardiac output was 2.0 L/min with a flow pulsatility range of approximately 4 L/min. In the low support experimental conditions (ID3), during diastole and systole the LVP and AOP ranged between −5 mmHg and 85 mmHg, and between 40 mmHg and 92 mmHg, respectively. The mean total cardiac output was 2.2 L/min, however with a diminished flow pulsatility range

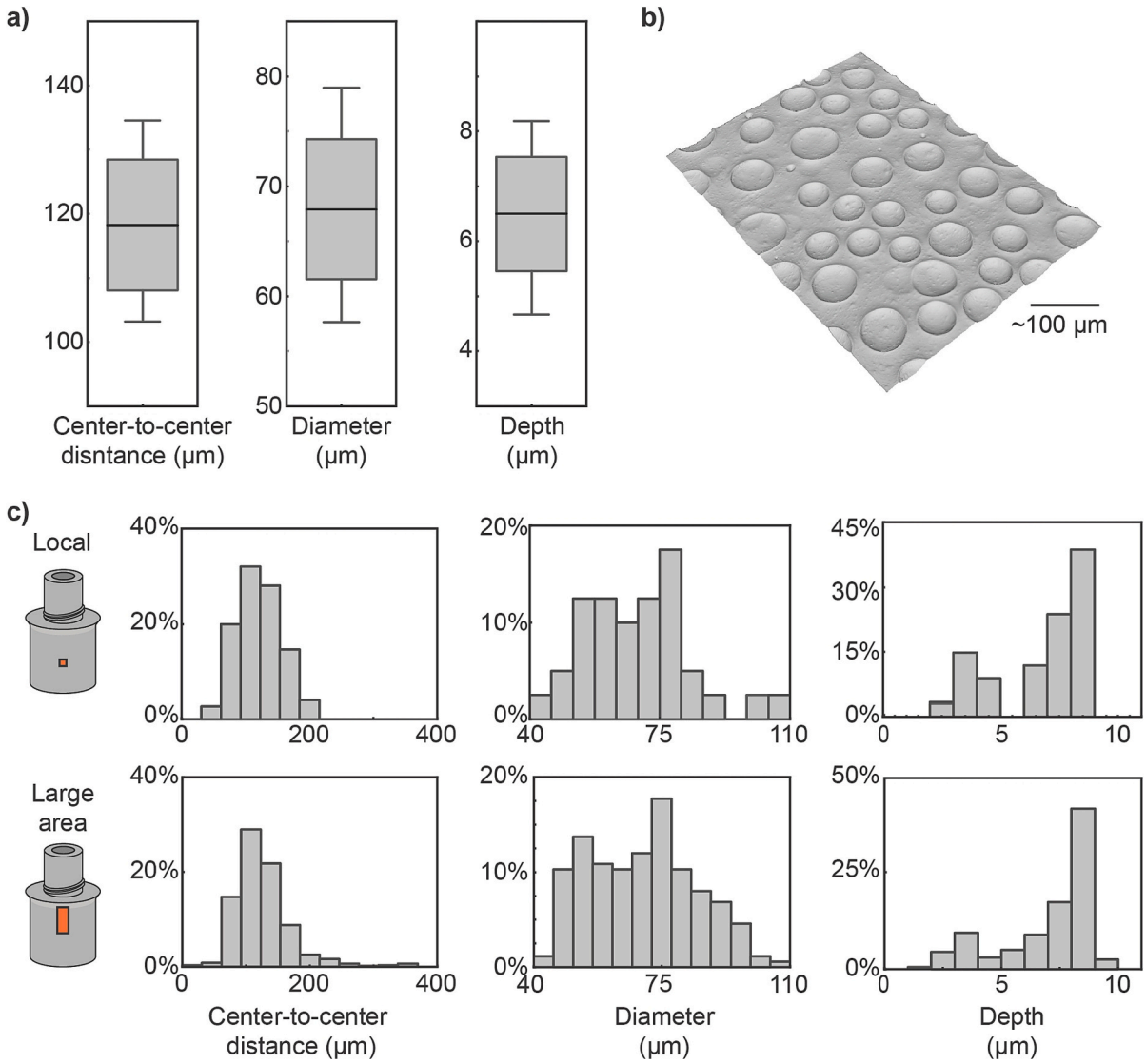

Fig. 6. Overview of the surface topography characterization. **a)** Summary of mean center-to-center distance, diameter, and depth of the wells. The box stands for standard deviation (SD) and the whiskers cover 5–95 % of the data. **b)** Representative image of a local scan area. **c)** Histograms of the parameter distributions for a local scan (upper panels) and a large area scan (stitched from 50 (2 × 25) local scans, lower panels).

of approximately 1 L/min.

3.3. Endothelial retention

The efficacy of the seeding protocol described in Section 2.3 and the ability of ECs to form a complete monolayer on the complex cylindrical surface of a commercial IC was tested under static culture in the incubator. As shown in Fig. 7a-b, three days after seeding, the convex outer surface of the cannula, where the BF topography was applied, was fully covered by ECs. VE-cadherin and actin staining also revealed the presence of a fully connected and mature monolayer.

Considering the necessary manipulations to attach the VAD on the heart phantom, as well as to mount the heart phantom with the integrated VAD on the rest of the setup, a high risk of mechanical damage on the EC monolayer was identified. The dismounting process to isolate the silicon layer with the ECs at the end of each experiment involves similar manipulations and thus risks. To quantify the effect of these manipulations on the integrity of the monolayer, the mounting and integration steps were performed, and after dismounting the monolayer retention was assessed. As shown in Fig. 7c-d, the IC surface presented signs of mechanical damage, highlighted by areas in which cells were connected through VE-cadherin-positive junctions intermingled with areas where cells were not present (Fig. 7d). This indicates that the mounting/dismounting process performed for all experiments prior the implementation of the support scenario under investigation compromised the quality of the monolayer by 44 %.

Additionally, since the experiments were conducted for 8 h on a complex, large-scale setup that requires controlled temperature and CO_2 administration, the risk of a compromised environment for the ECs increases. To assess the effect of such an environment on the endothelial retention and allow a better evaluation of ECs adaptation under varying hemodynamic conditions, the IC was mounted in the realistic heart phantom and remained in static conditions for 8 h. In Fig. 7f-g, it can be seen that during this experimental setting, besides areas with signs of mechanical damages, areas with retracted ECs could be identified, as highlighted by the presence of cells in confluent conditions without VE-cadherin properly localized at cell-cell contacts (Fig. 7g, lower panels). Hence, the prolonged incubation of the ECs in the unique environment developed inside the setup resulted in further impaired endothelial retention, reducing the IC surface with a high-quality EC monolayer to 52 %.

After quantifying the influence of the procedural steps, the retention of the endothelial monolayer experiencing low pulsatility conditions with (ID3, Table 1) and without the VAD support (ID1, Table 1) was analyzed. As depicted in Fig. 8a-b, compared to the static setup counterpart, the flow phenomena developed during the low pulsation without the VAD support setting, did not significantly reduce the percentage of the IC surface covered by a fully connected monolayer, but they did increase significantly ($p = 0.020$) that of cell denudation. The altered flow and pressure conditions in the vicinity of the IC by the addition of VAD support, significantly decreased ($p = 0.011$) the area where a connected monolayer was present by 26 % (compared to the static setup experiment) and, subsequently, increased significantly ($p = 0.002$) that of cell denudation.

Finally, to correlate the quality of the monolayer with the position of the IC and the surrounding tissue inside the heart phantom, the quality-maps of the EC monolayers (presented in Figs. 7 and 8) were integrated in the 3D CAD model of the IC. Four complementary fields of view of the 3D CAD model of the IC being positioned on the apex of the heart phantom are demonstrated in Fig. 9. In region 1 of this figure, where a complex of papillary muscles is near to the IC, a narrow area without any cells is detected in the static setup experiment (Fig. 9c), which however is not evident in the low pulsation experiment (Fig. 9d). In region 2, where a large part of papillary muscles is in close proximity with the IC, a big area where cells are detached is observed when focusing on the experiment with low pulsation (ID1) (Fig. 9d), in which the heart phantom is beating moderately. In region 3, relatively close to the IC there is another part of papillary muscles and a small area without any cells can be identified in both experimental conditions. Lastly, in region 4, no major differences in terms of EC retention regarding the position of the IC inside the heart phantom were observed comparing the static setup experiment (ID0) (Fig. 9c) with the experiment with low pulsation without VAD support (ID1) (Fig. 9d). In all views of Fig. 9, it can be observed that the lower region of the IC, which is prone to stagnation and thus thrombus formation, is covered with a full EC monolayer.

4. Discussion

The generation of an adaptive and durable interface to protect non-resorbable implant materials – the so-called foreign body – from the interaction with the surrounding cells and tissues, holds the promise to minimize or eliminate post-implantation complications. These range from fibrotic encapsulation of soft tissue implants or metallic implants such as pacemakers [34,35] to the activation of blood coagulation at the interface with devices that are in direct contact with blood [36]. Adverse body reactions can reduce the implant lifetime, promote device infection and can present a serious threat to the recipient [3]. The large foreign body surface area of contemporary VADs remains a vital challenge. The long-term and flawless integration of a VAD within the cardiovascular system would help to reduce the number of AEs and hence directly affect quality of life and eventually improve survival.

The human endothelium is naturally developed to interact with blood, and it is therefore obvious to consider endothelialization as the ideal solution to minimize VAD-related thrombotic events [37]. Yet, the functional and architectural complexity of the device, the delicate implantation procedure, and the inflammatory state of the human recipient, render the translation of promising endothelialization protocols a formidable challenge [37]. In this work, to investigate the translational hurdles of device endothelialization, a dedicated experimental setup (Fig. 3b) was developed. This *in-vitro* setup, by incorporating a VAD and a beating heart phantom that replicates the human heart anatomy (Fig. 3a), allows the simulation of flow and pressure phenomena that occur clinically after implantation. Multiple scenarios can be examined by adjusting the contraction of the heart phantom and, hence the level of pulsatility, as well as the support level provided by the VAD by modulating its speed profile (Fig. 4). The investigated scenarios represent a fraction of the possibilities provided by the custom-designed setup and modifications in the settings can lead to further experimental conditions. This allows the investigation of the hemodynamic conditions that accurately emulate clinically relevant scenarios.

This experimental setup is deployed to enable the investigation of the feasibility of IC endothelialization, as well as the assessment of the complementary surface modification techniques, in a bottom-up protective approach. In detail, the rational engineering modifications of implant surfaces in contact with blood with micron-scale topographical features [19] aims at generating geometrical elements that interact with the blood flow to mitigate the local hemodynamic conditions created by the VAD function and the heart movement [14]. This provides a viable substrate for the generation and maintenance of functional endothelia far beyond the physiological values of wall shear stress (WSS) of 5 Pa [24,26,29]. However, the implementation of such features in convoluted structures requires a free-form patterning approach, introduced by the BF patterning technology [28]. The BF patterning targeted the outer surface of the IC, where thrombus formation was commonly found in explanted hearts (Fig. 1). The application of the BF pattern on this specific area of the IC required the modification and optimization of the existing patterning protocol [28], to address the inherent complexity of the cylindrical IC surface and the different thermal properties of titanium. The successful adaptation of the fabrication protocol to the geometry and material characteristics of the IC of the HM3 VAD (Figs. 2 and 6) represents the first, crucial validation step that demonstrates feasibility of this approach on realistic implants, with the possibility to

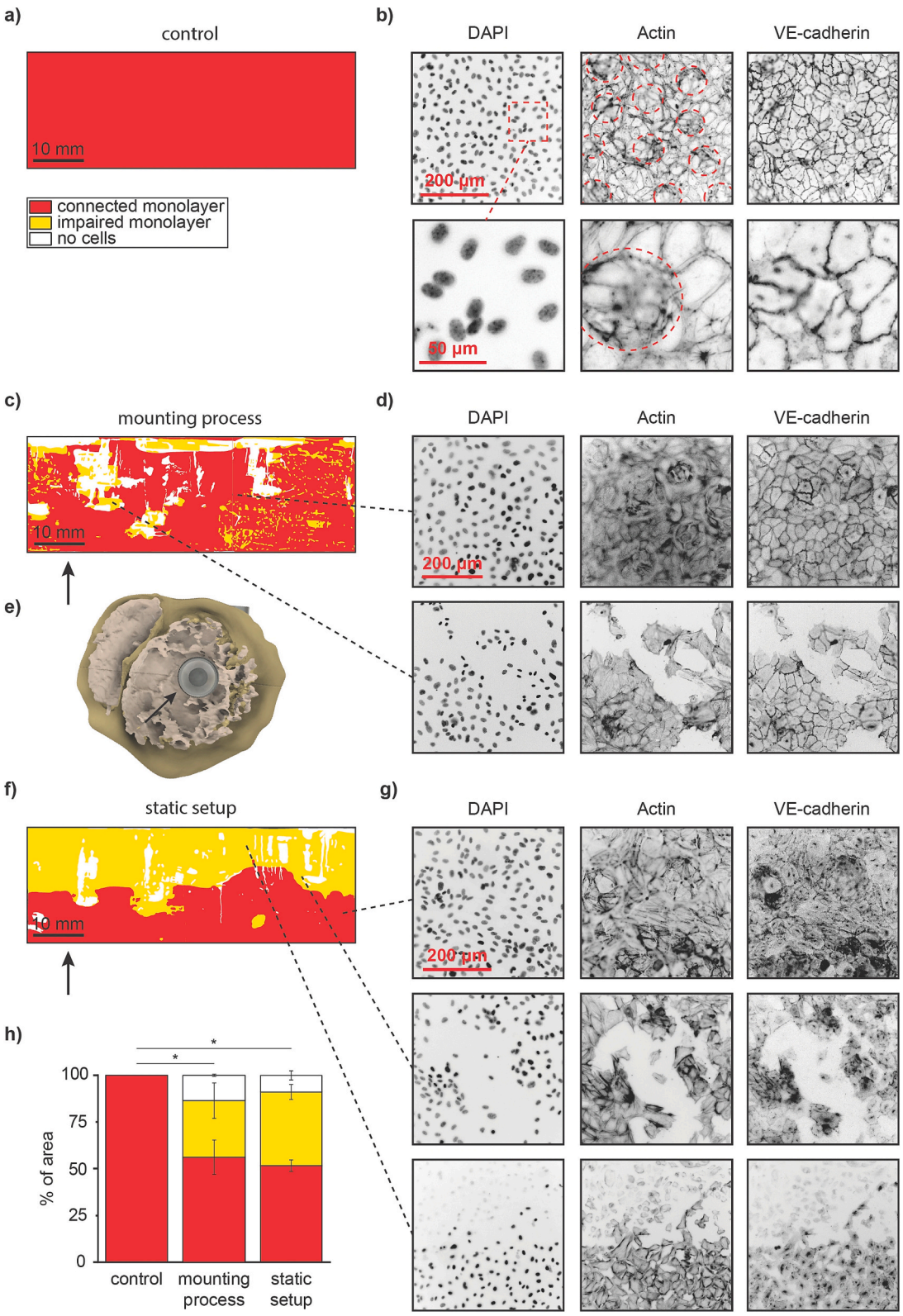

Fig. 7. Analysis of the endothelial cells on the inflow cannula (IC) in static conditions. **a)** Representative quality-map of recovered surface of control experiment. **b)** Representative images of DAPI, Actin and VE-cadherin in static experiment, connected monolayer (upper panels), magnified view (lower panels). The well profiles of the BF topography are indicated by red dashed circles. **c)** Representative quality-map of recovered surface of mounting experiment. **d)** Representative images of DAPI, Actin and VE-cadherin in mounting experiment, connected monolayer (upper panels), mechanically damaged monolayer (lower panels). **e)** Section view of the heart phantom (Fig. 9) with the integrated IC, at a plane parallel to the IC face. **f)** Representative quality-map of recovered surface of static experiment. **g)** Representative images of DAPI, Actin and VE-cadherin in static experiment, connected monolayer (upper panels), mechanically damaged monolayer (middle panels) and retracted cells (lower panels). **h)** Quantification of the recovered area, shown in percentage of areas in which the monolayer is connected, impaired or there are no cells. Bar graphs represent the mean, while error bars visualize the standard error of the mean (SEM). $n_{control} = 5$, $n_{mounting\ process} = 3$, $n_{static\ setup} = 3$, * $p < 0.05$, between all conditions ('connected monolayer', 'impaired monolayer', and 'no cells').

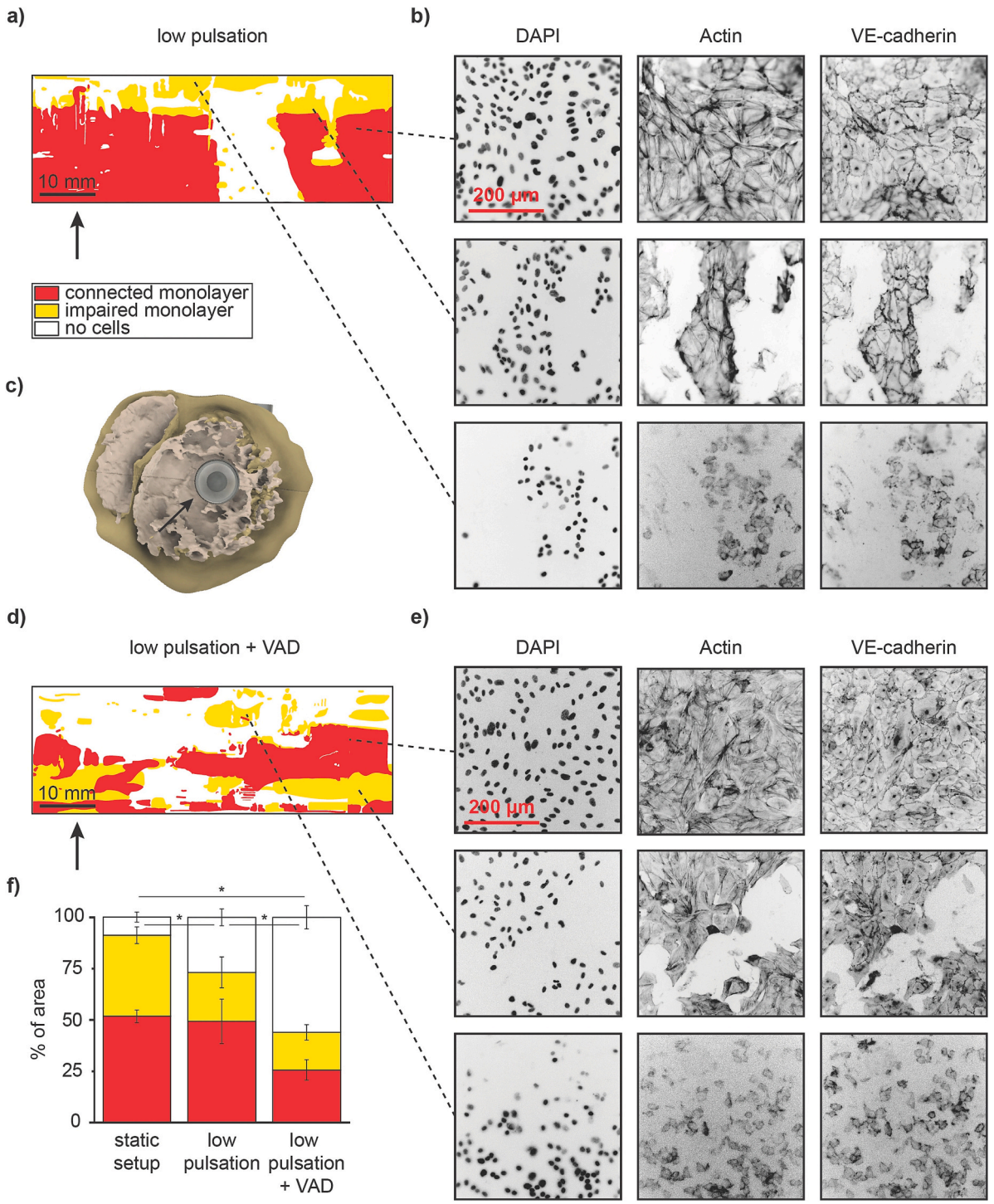

Fig. 8. Analysis of the response of the endothelial cells on the inflow cannula (IC) to flow phenomena inside the heart phantom. **a)** Representative quality-map of recovered surface of experiment with low pulsation. **b)** Representative images of DAPI, Actin and VE-cadherin in experiment with low pulsation, connected monolayer (upper panels), mechanically damaged monolayer (middle panels) and retracted cells (lower panels). **c)** Section view of the heart phantom (Fig. 9) with the integrated IC, at a plane parallel to the IC face. **d)** Representative quality-map of recovered surface of experiment with low pulsation and VAD actuation with rotational speed at 4000 rpm. **e)** Representative images of DAPI, Actin and VE-cadherin in experiment with low pulsation and VAD actuation with rotational speed at 4000 rpm, connected monolayer (upper panels), mechanically damaged monolayer (middle panels) and retracted cells (lower panels). **f)** Quantification of the recovered area, shown in percentage of areas in which the monolayer is connected, impaired or there are no cells. Bar graphs represent the mean, while error bars visualize the standard error of the mean (SEM). $n_{\text{static setup}} = 3$, $n_{\text{low pulsation}} = 3$, $n_{\text{low pulsation+VAD}} = 3$, * $p < 0.05$, for all conditions ('connected monolayer', 'impaired monolayer', and 'no cells') between static setup and low pulsation + VAD, * $p < 0.05$ for 'no cells' condition between static setup and low pulsation, and between low pulsation and low pulsation + VAD.

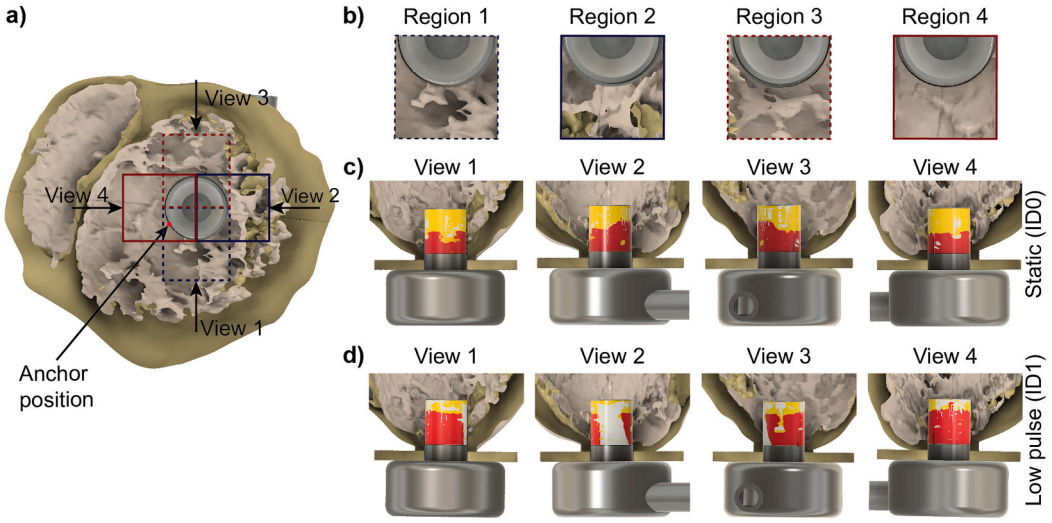

Fig. 9. Inflow cannula (IC) inside the heart phantom and its surrounding environment. **a)** Section view of the heart phantom with the integrated IC, at a plane perpendicular to the long axis of the IC. The view angles (View 1–4) used for the retention analysis are illustrated with the solid vectors. **b)** Detailed depiction of the regions around the IC for each view angle, shown on a top-to-bottom view. **c)** Representative quality-map of recovered surface on the IC for a static setup experiment. **d)** Representative quality-map of recovered surface on the IC for an experiment with low pulsation. A movie showing the entire heart phantom IC configuration is available in the supplementary material.

upscale to larger surfaces and more complex architectures, including cylindrical and spherical curvatures and transitional regions between the two.

Another important translational aspect refers to the basal conditions of the endothelial cells and tissues of the implant recipient [38]. Cardiovascular patients typically offer a limited number of functional endothelial cells, due to the underlying chronic vascular inflammation and other comorbidities [38,39]. In these conditions, the available population of endothelial cells can be significantly compromised, therefore tainting the success of endothelialization procedures [31,38]. A second important validation step, which was enabled by the developed experimental setup, besides the application of the topography on the IC, involves the endothelialization procedure and how to seed cells on a non-planar target substrate. The efficiency of this process and the number of cells required to obtain a functional and connected monolayer, provide essential information to identify the initial amount and quality of the homologous cells that should be derived from the patient to ensure successful endothelialization of the outer surface of the IC.

Among the most critical steps in the translation of any envisioned *in-vitro* endothelialization procedure [37] can be considered the handling and implantation process of the endothelialized VAD in an operating room environment. In this phase, the endothelium is exposed to environmental (temperature, humidity, and pH) and mechanical stresses. This is particularly relevant for the IC that is inserted at the apex area of any of the ventricles and, hence, it can be in direct contact with the papillary muscles. The movement of the papillary muscles caused by the beating heart, can result in excessive regional ECs removal, depending on the position and orientation of the IC and the anatomical characteristics of the heart. We have carefully reproduced all these aspects in our experiments to show that, indeed, most of the endothelial coverage loss is due to mechanical damage, or wounding, from the insertion and the removal of the IC during the mounting and dismounting processes, respectively (~44 % of the total area). The VAD actuation significantly impacts the remaining tissue on the IC, resulting to a fully connected monolayer only at the 26 % of the IC surface after the 8 h long experiments. However, in the long term, the parts of the IC surface in which the EC monolayer is damaged can be covered through the wound healing process [40]. Notably, larger areas of EC denudation were observed in the part of the IC that was in close proximity with a large part of heart phantom tissue only when the heart phantom was beating, while smaller areas of EC denudation near to complexes of papillary muscles were identified in both analyzed experiments (ID0 and ID1). These results indicate that during the mounting process the IC gets in contact with specific parts of the heart phantom, which are not always the same, and that the pulsation of the heart phantom further increases the contact of the IC with the heart phantom, leading to limited or extended damage on the EC monolayer. Additionally, the retention of the EC monolayer was higher in the lower part of the IC, which is more susceptible to thrombus formation. The importance of these results is therefore twofold, (1) providing a clear indication of critical steps in the envisioned clinical protocols regarding the positioning of the IC inside the heart based on the geometrical characteristics of the heart, and (2) pointing to the requirement of dedicated engineering tools for the frictionless insertion of the inflow cannula, aimed at preserving the endothelial lining.

Although important information regarding the feasibility of IC endothelialization was revealed, this work has several limitations. First, the presented results are susceptible to variations related to the manual insertion and removal of the IC of the VAD in and out of the heart phantom and the handling related to the mounting of the heart phantom with the VAD to the rest of the setup. This handling-induced variability, however, can be considered similar to the *in-vivo* procedure, in which the VAD positioning can be strongly affected by the anatomical position of the heart and the expertise of the surgeon [14]. Second, the experimental setup is fully compatible with patient-specific experiments, in which the endothelialization performance of a population of cells obtained from a vascular biopsy is evaluated in the frame of potential qualification to the procedure [41], however, no patient specific endothelial cells were used in the conducted experiments. Although this would provide a more reliable model of the cell population realistically available for an endothelialization procedure [38,41,42], such an approach would drastically increase the cost and complexity of the experimental procedure in this initial step of investigation, it could however be followed in further experimentation. Additionally, the duration of the flow experiments is intrinsically limited to 8 h in acute settings. This, however, does not diminish the value of the information retrieved in the phases of implant preparation, deployment, and initial actuation. Long term experiments of several days would add enormous complexity and relatively little value to the testing system, as they would not eliminate the need of chronic implantation during *in vivo* animal trials. In addition, it should be noted that the current setup of the beating

heart phantom does not account for the twisting motion observed in a healthy native heart, which may impact the flow dynamics and the interaction between the papillary muscle and the IC cannula. Nevertheless, it is important to highlight that the twisting motion is significantly reduced in a dilated heart that requires VAD support [43]. Therefore, the potential impact of the omitted motion on the accuracy of the obtained results is considered negligible. Last but not least, the generated total cardiac output was in the range of 2.5 L/min, imitating low activity levels (*e.g.*, sleeping conditions). However, further investigations including the development of flow conditions of approximately 5 L/min should be also performed to allow the assessment of the effect of the flow phenomena at rest conditions of the patient on the EC retention.

The investigation at hand is focused on an *ex-vivo* endothelialization approach in which human endothelial cells are seeded on the target substrate before the implantation of the VAD. This sequence is necessary due to the absence of alternative cellular sources, such as circulating progenitor cells and neighboring tissues at the site of implantation in the *in-vitro* experimental setup. However, the technologies and their demonstrated integration can be equally applied to alternative strategies aimed at the *in-vivo* (*i.e.*, post implantation) generation of a protective endothelial tissue. The surface topography can be utilized with additional chemical functionalization to promote the docking and adhesion of circulating progenitor cells, together with the mobilization of adult ECs from neighboring tissues to cover the open space [44]. While the extent of the coverage that can be obtained through *in-vivo* endothelialization remains to be defined, such protocols bypass the technical difficulties related to the *ex-vivo* handling of human cells and consequently reduce the regulatory concerns that may hinder the clinical translation of endothelialization procedures.

5. Conclusions

The endothelialization of VAD interfaces that are in contact with blood holds the promise of a better hemocompatibility and can be the cornerstone for the minimization of VAD-related thrombotic events. This proof-of-concept study reports a novel experimental setup that allows the investigation and validation of surface modification and endothelialization approaches in large-scale. Based on this setup, this work provides evidence that the application of micron-scale topographical features and the endothelialization of the outer surface of the inflow cannula of a state-of-the-art VAD is feasible. The efficacy of these approaches has been validated against physiologic hemodynamic conditions, also considering the effect of handling and implantation processes on the translation of this approach in the clinical environment.

Supplementary data to this article can be found online at https://doi.org/10.1016/j.bioadv.2023.213485.

CRediT authorship contribution statement

Konstantinos Magkoutas: Conceptualization, Methodology, Software, Validation, Formal analysis, Investigation, Visualization, Writing – original draft. **Nafsika Chala:** Conceptualization, Methodology, Software, Validation, Formal analysis, Investigation, Visualization, Writing – original draft. **Xi Wu:** Methodology, Software, Validation, Formal analysis, Investigation, Visualization, Writing – original draft. **Dimos Poulikakos:** Writing – review & editing, Supervision, Funding acquisition. **Edoardo Mazza:** Writing – review & editing, Supervision, Funding acquisition. **Mirko Meboldt:** Writing – review & editing, Supervision, Funding acquisition. **Volkmar Falk:** Writing – review & editing, Supervision, Funding acquisition. **Aldo Ferrari:** Conceptualization, Writing – original draft, Supervision, Funding acquisition. **Costanza Giampietro:** Conceptualization, Writing – original draft, Supervision, Funding acquisition. **Marianne Schmid Daners:** Conceptualization, Writing – review & editing, Supervision, Funding acquisition.

Declaration of competing interest

Xi Wu, Edoardo Mazza, and Aldo Ferrari have patent #WO2022/106290A1 issued to ETH ZURICH.

Data availability

Data will be made available on request.

Acknowledgments

This work is part of the Zurich Heart project under the umbrella of "Hochschuldmedizin Zurich". It is financially supported by the Stavros Niarchos Foundation (SNF) and the Swiss National Science Foundation (grant SNF; 205321_188828). We thank Gianna Klucker (ETH Zurich) for her help and Friedrich Kaufmann (German Heart Center Berlin) for providing the image of the explanted inflow cannula of the HeartMate 3.

References

[1] M.T. Cain, M.S. Firstenberg, J.C.C. Jr, Heart transplant and ventricular assist: cardiac surgery and heart failure perspective, US Cardiology Review 15 (e16) (2021) 2021.
[2] C.A. Theochari, G. Michalopoulos, E.K. Oikonomou, S. Giannopoulos, I. P. Doulamis, M.A. Villela, D.G. Kokkinidis, Heart transplantation versus left ventricular assist devices as destination therapy or bridge to transplantation for 1-year mortality: a systematic review and meta-analysis, Ann Cardiothorac Sur 7 (1) (2018) 3–+.
[3] E.J. Molina, P. Shah, M.S. Kiernan, W.K. Cornwell III, H. Copeland, K. Takeda, F. G. Fernandez, V. Badhwar, R.H. Habib, J.P. Jacobs, The society of thoracic surgeons intermacs 2020 annual report, Ann. Thorac. Surg. 111 (3) (2021) 778–792.
[4] R.L. Kormos, J. Cowger, F.D. Pagani, J.J. Teuteberg, D.J. Goldstein, J.P. Jacobs, R. S. Higgins, L.W. Stevenson, J. Stehlik, P. Atluri, The Society of Thoracic Surgeons Intermacs database annual report: evolving indications, outcomes, and scientific partnerships, J. Heart Lung Transplant. 38 (2) (2019) 114–126.
[5] A. Petrou, J. Lee, S. Dual, G. Ochsner, M. Meboldt, M. Schmid Daners, Standardized comparison of selected physiological controllers for rotary blood pumps: in vitro study, Artificial Organs 42 (3) (2018) E29–E42.
[6] J.J. Han, M.A. Acker, P. Atluri, Left ventricular assist devices: synergistic model between technology and medicine, Circulation 138 (24) (2018) 2841–2851.
[7] M.P. Weber, J. Stulak, S. Maltais, F.D. Pagani, J. Cowger, V. Tchantchaleishvili, Quality of life metrics in LVAD patients after hemocompatibility-related adverse events, Artif. Organs 46 (8) (2022) 1616–1625, https://doi.org/10.1111/aor.14235.
[8] R.L. Kormos, C.F. Antonides, D.J. Goldstein, J.A. Cowger, R.C. Starling, J. K. Kirklin, J.E. Rame, D. Rosenthal, M.L. Mooney, K. Caliskan, Updated definitions of adverse events for trials and registries of mechanical circulatory support: a consensus statement of the mechanical circulatory support academic research consortium, J. Heart Lung Transplant. 39 (8) (2020) 735–750.
[9] M.R. Mehra, The burden of haemocompatibility with left ventricular assist systems: a complex weave, Eur. Heart J. 40 (8) (2019) 673–677.
[10] J.J. Teuteberg, J.C. Cleveland Jr., J. Cowger, R.S. Higgins, D.J. Goldstein, M. Keebler, J.K. Kirklin, S.L. Myers, C.T. Salerno, J. Stehlik, The Society of Thoracic Surgeons Intermacs 2019 annual report: the changing landscape of devices and indications, Ann. Thorac. Surg. 109 (3) (2020) 649–660.
[11] N. Uriel, P.C. Colombo, J.C. Cleveland, J.W. Long, C. Salerno, D.J. Goldstein, C. B. Patel, G.A. Ewald, A.J. Tatooles, S.C. Silvestry, Hemocompatibility-related outcomes in the MOMENTUM 3 trial at 6 months: a randomized controlled study of a fully magnetically levitated pump in advanced heart failure, Circulation 135 (21) (2017) 2003–2012.
[12] A. Camaj, V. Fuster, G. Giustino, S.W. Bienstock, D. Sternheim, R. Mehran, G. D. Dangas, A. Kini, S.K. Sharma, J. Halperin, M.R. Dweck, M.E. Goldman, Left ventricular Thrombus following acute myocardial infarction JACC state-of-the-art review, J. Am. Coll. Cardiol. 79 (10) (2022) 1010–1022.
[13] C.H. Glass, A. Christakis, G.A. Fishbein, J.C. Watkins, K.C. Strickland, R. N. Mitchell, R.F. Padera, Thrombus on the inflow cannula of the HeartWare HVAD: an update, Cardiovasc. Pathol. 38 (2019) 14–20.
[14] G. He, L. Han, J.F. Zhang, A. Shah, D.J. Kaczorowski, B.P. Griffith, Z.J. Wu, Numerical study of the effect of LVAD inflow cannula positioning on thrombosis risk, Comput Method Biomec 25 (8) (2022) 852–860.
[15] F. Kaufmann, C. Hörmandinger, C. Knosalla, V. Falk, E. Potapov, Thrombus formation at the inflow cannula of continuous-flow left ventricular assist devices—a systematic analysis, Artif. Organs 46 (8) (2022) 1573–1584, https://doi.org/10.1111/aor.14222.
[16] K.C. Strickland, J.C. Watkins, G.S. Couper, M.M. Givertz, R.F. Padera, Thrombus around the redesigned HeartWare HVAD inflow cannula: a pathologic case series, J Heart Lung Transpl 35 (7) (2016) 926–930.
[17] M. Ghodrati, A. Maurer, T. Schloglhofer, T. Khienwad, D. Zimpfer, D. Beitzke, F. Zonta, F. Moscato, H. Schima, P. Aigner, The influence of left ventricular assist

device inflow cannula position on thrombosis risk, Artif. Organs 44 (9) (2020) 939–946.
[18] K.S. Lavery, C. Rhodes, A. Mcgraw, M.J. Eppihimer, Anti-thrombotic technologies for medical devices, Adv Drug Deliver Rev 112 (2017) 2–11.
[19] J. Kuchinka, C. Willems, D.V. Telyshev, T. Groth, Control of blood coagulation by Hemocompatible material surfaces-a review, Bioengineering (Basel) 8 (12) (2021).
[20] P. Kurtyka, R. Kustosz, M. Kaczmarek, M. Gonsior, K. Tokarska, Surface modifications for inflow cannulas of ventricular assist devices–comparison of latest solutions, Engineering of Biomaterials 22 (151) (2019).
[21] A. Ferrari, C. Giampietro, B. Bachmann, L. Bernardi, D. Bezuidenhhout, P. Ermanni, R. Hopf, S. Kitz, G. Kress, C. Loosli, V. Marina, M. Meboldt, G. Pellegrini, D. Poulikakos, M. Rebholz, M. Schmid Daners, T. Schmidt, C. Starck, G. Stefopoulos, S. Sündermann, B. Thamsen, P. Zilla, E. Potapov, V. Falk, E. Mazza, A novel hybrid membrane VAD as first step toward Hemocompatible blood propulsion, Ann. Biomed. Eng. 49 (2) (2021) 716–731.
[22] E. Dejana, F. Orsenigo, M.G. Lampugnani, The role of adherens junctions and VE-cadherin in the control of vascular permeability, J. Cell Sci. 121 (Pt 13) (2008) 2115–2122.
[23] M. Giannotta, M. Trani, E. Dejana, VE-cadherin and endothelial adherens junctions: active guardians of vascular integrity, Dev. Cell 26 (5) (2013) 441–454.
[24] B.J. Bachmann, C. Giampietro, A. Bayram, G. Stefopoulos, C. Michos, G. Graeber, M.V. Falk, D. Poulikakos, A. Ferrari, Honeycomb-structured metasurfaces for the adaptive nesting of endothelial cells under hemodynamic loads, Biomater Sci 6 (10) (2018) 2726–2737.
[25] E. Potthoff, D. Franco, V. D'Alessandro, C. Starck, V. Falk, T. Zambelli, J. A. Vorholt, D. Poulikakos, A. Ferrari, Toward a rational design of surface textures promoting endothelialization, Nano Lett. 14 (2) (2014) 1069–1079.
[26] F. Robotti, D. Franco, L. Banninger, J. Wyler, C.T. Starck, V. Falk, D. Poulikakos, A. Ferrari, The influence of surface micro-structure on endothelialization under supraphysiological wall shear stress, Biomaterials 35 (30) (2014) 8479–8486.
[27] G. Stefopoulos, C. Giampietro, V. Falk, D. Poulikakos, A. Ferrari, Facile endothelium protection from TNF-alpha inflammatory insult with surface topography, Biomaterials 138 (2017) 131–141.
[28] X. Wu, S. Moimas, R. Hopf, C. Giampietro, A. Kourouklis, V. Falk, E. Mazza, A. Ferrari, A free-form patterning method enabling endothelialization under dynamic flow, Biomaterials 273 (2021).
[29] F. Orsenigo, C. Giampietro, A. Ferrari, M. Corada, A. Galaup, S. Sigismund, G. Ristagno, L. Maddaluno, G.Y. Koh, D. Franco, V. Kurtcuoglu, D. Poulikakos, P. Baluk, D. McDonald, M. Grazia Lampugnani, E. Dejana, Phosphorylation of VE-cadherin is modulated by haemodynamic forces and contributes to the regulation of vascular permeability in vivo, Nat. Commun. 3 (2012) 1208.
[30] K. von Petersdorff-Campen, J. Abeken, D. de Zelicourt, V. Kurtcuoglu, M. Meboldt, M. Schmid Daners, In vitro testing and comparison of additively manufactured polymer impellers for the CentriMag blood pump, ASAIO J. 67 (3) (2021) 306–313.
[31] N. Chala, S. Moimas, C. Giampietro, X. Zhang, T. Zambelli, V. Exarchos, T. Z. Nazari-Shafti, D. Poulikakos, A. Ferrari, Mechanical fingerprint of senescence in endothelial cells, Nano Lett. 21 (12) (2021) 4911–4920.
[32] F. Adams, T. Qiu, A. Mark, B. Fritz, L. Kramer, D. Schlager, U. Wetterauer, A. Miernik, P. Fischer, Soft 3D-printed phantom of the human kidney with collecting system, Ann. Biomed. Eng. 45 (4) (2017) 963–972.
[33] Origin(Pro), Version, OriginLab Corporation: Northampton, MA, USA, 2019.
[34] N.G. Welch, D.A. Winkler, H. Thissen, Antifibrotic strategies for medical devices, Adv Drug Deliver Rev 167 (2020) 109–120.
[35] F. Robotti, I. Sterner, S. Bottan, J.M.M. Rodriguez, G. Pellegrini, T. Schmidt, V. Falk, D. Poulikakos, A. Ferrari, C. Starck, Microengineered biosynthesized cellulose as anti-fibrotic in vivo protection for cardiac implantable electronic devices, Biomaterials 229 (2020).
[36] I.H. Jaffer, J.C. Fredenburgh, J. Hirsh, J.I. Weitz, Medical device-induced thrombosis: what causes it and how can we prevent it? J. Thromb. Haemost. 13 (S1) (2015) S72–S81.
[37] S. Jana, Endothelialization of cardiovascular devices, Acta Biomater. 99 (2019) 53–71.
[38] B. Indranil, A.K. Gausal, Endothelial dysfunction in cardiovascular diseases, in: S. Kaneez Fatima, S. Seyed Soheil Saeedi, B. Nazar Luqman (Eds.), Basic and Clinical Understanding of Microcirculation 5, IntechOpen, Rijeka, 2019.
[39] S.I. Bloom, M.T. Islam, L.A. Lesniewski, A.J. Donato, Mechanisms and consequences of endothelial cell senescence, Nat. Rev. Cardiol. 20 (1) (2023) 38–51, https://doi.org/10.1038/s41569-022-00739-0.
[40] D. Franco, F. Milde, M. Klingauf, F. Orsenigo, E. Dejana, D. Poulikakos, M. Cecchini, P. Koumoutsakos, A. Ferrari, V. Kurtcuoglu, Accelerated endothelial wound healing on microstructured substrates under flow, Biomaterials 34 (5) (2013) 1488–1497.
[41] V. Exarchos, E. Zacharova, S. Neuber, C. Giampietro, S.E. Motta, H. Hinkov, M. Y. Emmert, T.Z. Nazari-Shafti, The path to a hemocompatible cardiovascular implant: advances and challenges of current endothelialization strategies, Frontiers in Cardiovascular Medicine (2022) 9.
[42] O. Tura-Ceide, V.F.E.D. Smolders, N. Aventin, C. Moren, M. Guitart-Mampel, I. Blanco, L. Piccari, J. Osorio, C. Rodriguez, M. Rigol, N. Solanes, A. Malandrino, K. Kurakula, M.J. Goumans, P.H.A. Quax, V.I. Peinado, M. Castella, J.A. Barbera, Derivation and characterisation of endothelial cells from patients with chronic thromboembolic pulmonary hypertension, Sci Rep-Uk 11 (1) (2021).
[43] M.J. Ranek, J.M. Berthiaume, J.A. Kirk, R.C. Lyon, F. Sheikh, B.C. Jensen, B. D. Hoit, J. Butany, M. Tolend, V. Rao, M.S. Willis, Chapter 5 - pathophysiology of heart failure and an overview of therapies, in: L.M. Buja, J. Butany (Eds.), Cardiovascular Pathology, Fifth edition, Academic Press, 2022, pp. 149–221.
[44] M. Tallawi, E. Rosellini, N. Barbani, M.G. Cascone, R. Rai, G. Saint-Pierre, A. R. Boccaccini, Strategies for the chemical and biological functionalization of scaffolds for cardiac tissue engineering: a review, J. R. Soc. Interface 12 (108) (2015) 20150254.